Elsevier Editorial System(tm) for Optics Communications
Manuscript Draft

Manuscript Number:

Title: Analysis of bit rate dependence up to 80 Gbit/s of a simple wavelength converter based on XPM in a SOA and a shifted filtering

Article Type: Journal Article

Section/Category: II. Optical information and image processing

Keywords:

Corresponding Author: Dr Gwenaelle Girault, Ph.D

Corresponding Author's Institution: Foton

First Author: Gwenaelle Girault, PhD

Order of Authors: Gwenaelle Girault, PhD; Aisling M Clarke, PhD; Douglas Reid, PhD; Celine Guignard, PhD; Laurent Bramerie, PhD; Prince Anandarajah, PhD; Liam P Barry, Professor; Jean-Claude Simon, Professor; John Harvey, Professor

Manuscript Region of Origin:

Abstract: This paper provides the analysis of wavelength converted pulses obtained with a simple semiconductor optical amplifier (SOA)-based wavelength conversion scheme, which exploits cross phase modulation (XPM) in an SOA in conjunction with shifted filtering. The analysis includes experimental measurements of the back-to-back system performances as well as frequency-resolved optical gating (FROG) characterisations of the wavelength converted pulses. These measurements are implemented at different bit rates up to 80 Gbit/s and for both red and blue shifted filtering, particularly showing different patterning effect dependences of red and blue shifting techniques. This analysis is developed by the addition of a numerical study which corroborates the experimental results. A further understanding of the different performances of red and blue filtering techniques, presented in the literature, can thus be proposed. The placement of the filter to undertake red shifted filtering (RSF) allows us to achieve very short pulse

widths but high bit rate operation is limited by pattern effects. The blue shifted filtering (BSF) technique shows optimum performance as regards to patterning effects even if the wavelength converted pulses can be larger.

Analysis of bit rate dependence up to 80 Gbit/s of a simple wavelength converter based on XPM in a SOA and a shifted filtering

G. Girault[1], A. M. Clarke[2], D. Reid[2], C. Guignard[2], L. Bramerie[1], P. Anandarajah[2], L. P. Barry[2], J-C. Simon[1], J. Harvey[3]

[1]Persyst Platform, CNRS Foton-Enssat, University of Rennes, Lannion, France

[2] RINCE, School of Electronic Eng., Dublin City University, Ireland

[3] Physics Dept., Auckland University, New Zealand

Corresponding author:
G. Girault, girault@enssat.fr,
Persyst Platform, CNRS Foton-Enssat, 6, rue de Kerampont, BP 80518, 22305 Lannion cedex, FRANCE.
phone: +33 (0)2 96 46 91 04, fax: +33 (0)2 96 46 90 76

Pacs: 42.15.Eq Optical system design,
42.55.Px Semiconductor lasers; laser diodes,
42.60.Da Resonators, cavities, amplifiers, arrays, and rings,
42.60.Jf Beam characteristics: profile, intensity, and power; spatial pattern formation,
42.65.Re Ultrafast processes; optical pulse generation and pulse compression
42.81.Uv Fiber networks
81.05.Ea III–V semiconductors

Keywords: All-optical switch, Frequency-resolved optical gating, Semiconductor optical amplifier, Shifted bandpass filtering, Wavelength conversion, Ultrafast

Abstract This paper provides the analysis of wavelength converted pulses obtained with a simple semiconductor optical amplifier (SOA)-based wavelength conversion scheme, which exploits cross phase modulation (XPM) in an SOA in conjunction with shifted filtering. The analysis includes experimental measurements of the back-to-back system performances as well as frequency-resolved optical gating (FROG) characterisations of the wavelength converted pulses. These measurements are implemented at different bit rates up to 80 Gbit/s and for both red and blue shifted filtering, particularly showing different patterning effect dependences of red and blue shifting techniques. This analysis is developed by the addition of a numerical study which corroborates the experimental results. A further understanding of the different performances of red and blue filtering techniques, presented in the literature, can thus be proposed. The placement of the filter to undertake red shifted filtering (RSF) allows us to achieve very short pulse widths but high bit rate operation is limited by pattern effects.

The blue shifted filtering (BSF) technique shows optimum performance as regards to patterning effects even if the wavelength converted pulses can be larger.

1 Introduction

With ever increasing demand for high-bandwidth applications, the growth towards implementing Tbit/s optical networks continues. Wavelength division multiplexing (WDM) is currently the optical multiplexing technique of choice in order to exploit the large bandwidth capabilities provided by optical fibre. As individual bit rates increase, all-optical processing techniques will be required to provide simple network management.

In particular, wavelength converters will be key elements of optical networks, in that they enable simpler network operation and provide dynamic provisioning in order to make full use of the available bandwidth [1, 2]. Presently individual channel rates do not exceed 40 Gbit/s, however the bit rate of each individual line is set to increase to even greater capacities. Therefore there is a need to design and develop all-optical wavelength converters that can perform at bit rates greater than 40 Gbit/s.

Future all-optical wavelength converters must meet certain criteria such as simple and stable operation, cost effectiveness and low energy consumption. A semiconductor optical amplifier (SOA) is a candidate which meets all of the above criteria [3]. In addition these components have a small footprint, hold possibilities for monolithic integration [4], polarisation insensitivity [5], and exhibit high nonlinearities for low input powers (compared to nonlinearities in fibres). Thus SOAs are ideal candidates for use as ultrafast wavelength converters [6, 7].

One method of implementing wavelength conversion with SOAs is to use cross gain modulation (XGM). However the main disadvantages of this process are the polarity inversion of the output data in comparison to the input signal, the poor output extinction ratio and the bit rate limitation due to the SOA gain recovery time which can typically vary from

40-100's ps for different SOAs [8]. A solution to overcome these disadvantages is to use cross phase modulation (XPM) in a SOA in conjunction with an interferometer [9-11]. However such schemes are often complicated and generally display problems with stability for example due to polarisation sensitivity. A simpler technique is to use a shifted bandpass filter (BPF) following the SOA. This was first proposed by Ellis *et al.* [12] and has recently shown to operate at very high bit rates by Liu *et al.* [13]. This solution overcomes the limitation due to the slow gain recovery time of SOAs and improves the extinction ratio in comparison with simple XGM. However the output data polarity is still inverted and the extinction ratio is insufficient. Cho *et al.* [14] presented a similar scheme but the proposed setup preserves the polarity of the input data by spectrally shifting the filter further from the continuous wave probe signal, thus primarily exploiting XPM in the SOA, in the same way as using phase modulation in a fibre associated with a shifted filter [15, 16]. This kind of device gives an enhanced extinction ratio and has enabled operation at high bit rates [17]. Fu *et al.* [18] have experimentally characterised the evolution of the wavelength converted pulse shape as the filter is shifted toward either longer (red) or shorter (blue) wavelengths at a bit rate of 10 Gbit/s. At this bit rate, Chayet *et al.* [19] have demonstrated the regenerative properties of such a scheme based on a high wavelength (red shifted) filtering. However these papers do not consider the dependence of the wavelength converted pulses for both blue and red shifting techniques on the increasing bit rate. In order to achieve high bit rate performances, the addition of an interferometer to the bandpass filter in order to optimize the filtering has also been proposed [20, 21] achieving wavelength conversion up to 160 Gbit/s [22, 23]. However the use of an interferometer impacts negatively the stability and the simplicity of the device. Finally a promising scheme has recently been proposed [24], coupling two bandpass filters, respectively red and blue shifted, but the demonstrated bit rate did not exceed 40 Gbit/s up to now.

In this paper we present an analysis of wavelength converted pulses obtained with a simple scheme which primarily exploits XPM in an SOA in conjunction with a shifted BPF. This scheme offers the advantages of simplicity, polarisation insensitivity, stability, polarity preservation and large output extinction ratio. The analysis investigates the scheme in terms of performance up to bit rates of 80 Gbit/s and examines the output pulse and chirp profiles dependent on the repetition rate of the wavelength converted pulses and on the placement of the shifted filter to conserve either red or blue spectral components.

The paper is organized as follows: Section 2 describes the principle of the studied wavelength converter. Section 3 presents the back-to-back bit error rate (BER) performances of the wavelength conversion scheme and analyzes their temporal and chirp output profiles using frequency-resolved optical gating (FROG) measurements at increasing repetition rates up to 80 GHz. Section 4 proposes a numerical support to the experimental study in order to bring a full understanding of the wavelength converter behaviour.

2 Principle of the wavelength converter

The principle of the SOA and filter-based wavelength converter, which is illustrated in Fig. 1, consists of injecting two signals into the SOA: The modulated data signal at wavelength λ_1 and a simple continuous wave (CW), called a "probe", at the required conversion wavelength, λ_2.

The input data signal modulates the gain in the SOA due to gain saturation. In the same way the refractive index and thus the phase of the probe are also modulated. This process of XPM causes a shift of the probe spectral components firstly to longer wavelengths, known as red-shifting and then to shorter wavelengths known as blue-shifting. Fig. 2 is an illustrative view of the corresponding temporal effects between an input pump pulse, the dynamic SOA gain compression and the frequency shift induced by the SOA, *i.e.* the SOA 'chirp'.

Generally a BPF is placed after the SOA, to reject the original input data signal. By shifting this filter off centre to select the red shifted or blue-shifted spectral components of the probe signal, the limitations typically governed by the slow gain recovery time of the SOA can be overcome, taking advantage of the short time scale on which the chirp occurs [22]. If the filter is placed further to longer or shorter wavelengths so as to suppress the spectral component of the probe at λ_2, the phase modulation of the probe signal can be converted into intensity modulation and thus the polarity of the input signal can be preserved [15, 17]. This can be explained in further detail: When a low energy pulse ('0') enters the SOA, there is no saturation of its gain and thus there is no corresponding wavelength shift of the probe spectral components. Thus the filter rejects the CW probe signal. On the contrary when a high energy pulse ('1') enters the SOA, the probe spectral components are first shifted towards the longer wavelengths (red shift) and then to shorter wavelengths (blue shift). Thus depending on the filter bandpass either the red or blue shifted spectral components are maintained while the other probe spectral components (including the central component at λ_2) are suppressed.

The power efficiency of this technique increases as the amount of induced spectral broadening (*i.e.* 'chirp') becomes larger. Therefore the shorter and more energetic the input pulses are, the more efficient the process is, particularly thanks to intra-band effects [25]. In addition the more suppressed the central component of the probe (at λ_2) is, the larger is the output extinction ratio. Therefore, on one hand, if the input probe power is high, the used filter has more difficulties in rejecting the probe central component properly, and thus the extinction ratio is degraded. On the other hand, the gain recovery time is shorter [26] and the cross modulation processes are better. A trade-off must then be found on the input probe power. Finally we can also note that, as regards to the pump and probe wavelength detuning, the best way is to have a probe wavelength longer than that of the pump. In this case, the probe power can be significantly increased without too much limiting the gain compression

induced by the pump, which is a well-known result on XGM technique [6]. Moreover, the phase-amplitude coupling is then higher at the probe wavelength and the amount of induced chirp can therefore be greater [22].

3 Experimental observations

The aim of the following experimental study is the analysis of the behaviour of such a wavelength converter at different bit rates in the case of both blue-shifted filtering (BSF) and red-shifted filtering (RSF). The analysis consists of BER measurements versus received power and a pulse and chirp characterisation of the wavelength converted pulses at different bit repetition rates up to 80 GHz (10, 20, 40 and 80 GHz) to explore the wavelength converted signal dependence on its preceding pattern.

3.1 Experimental set up

The experimental set up is shown in Fig. 3. Mode-locked pulses with a full width at half maximum (FWHM) of 2.3 ps are generated at a repetition rate of 10 GHz and at a wavelength of 1545 nm. The pulses are amplified using an erbium doped fiber amplifier (EDFA) and passed through a Mach-Zehnder intensity modulator to obtain a 10 Gbit/s RZ-PRBS of length 2^7-1. The data signal is then passively multiplexed to the required bit rate of 10, 20, 40, or 80 Gbit/s. At 80 Gbit/s the average pulse power is 0 dBm (energy = 12.5 fJ,) and is reduced by 3 dB as the bit rate is decreased by half to maintain a constant pulse energy. The wavelength conversion scheme consists of injecting a CW signal coupled with the pump signal into an SOA. The probe power measured at the SOA input is 2.5 dBm. It ensures the best compromise between the processes speed and extinction ratio in our experiment, as it has been explained previously.

The measured slow gain recovery time of this SOA is 55 ps at a bias current of 250 mA. Two filters and an EDFA follow the SOA. The first filter is a fixed filter, the choice between

RSF or BSF is made by changing the probe wavelength rather than the position of the filter. Therefore to obtain optimised red and blue shifted filtering the probe signal is set at a wavelength of 1551.91 nm and 1558.6 nm respectively. This first filter has a sharp band edge, which is used to reject the original pump signal and to significantly reduce the CW portion of the probe. The second 3 nm tunable Gaussian filter is used to suppress further the CW signal and thus give an improved extinction ratio. An intermediate EDFA between the two filters is required to compensate for the high insertion loss due to the shifted filtering. The average power at the output of the wavelength converter is measured at approximately -2 dBm at 80 Gbit/s. Fig. 4 shows the signal spectra at the input of the wavelength converter, at the output of the SOA and after RSF and BSF.

3.2 Bit error rate measurements

To measure the BER, the signal was demultiplexed from 80 Gbit/s to 20 Gbit/s optically via two electro-absorption modulators and was then electrically demultiplexed to 10 Gbit/s. The power received level was measured at 20 Gbit/s just before the photodiode preceding the electrical demultiplexer. The BER measurements for both BSF and RSF at 80 Gbit/s are displayed in Fig. 5, in addition to a back-to-back measurement without wavelength conversion.

A BER of less than 10^{-9} was obtained at 80 Gbit/s with BSF as previously presented in [27]. A penalty of 2.5 dB compared to the back-to-back curve was observed at a BER of 10^{-9}. In contrast, the RSF technique only achieved a BER of less than 10^{-9} at 40 Gbit/s. Fig. 5 shows an error floor at a BER of 10^{-7} for 80 Gbit/s using RSF. This clearly highlights a different dependence on patterning effects between RSF and BSF techniques. The error floor present for the RSF technique is due to patterning effects as a consequence of the incomplete gain recovery of the SOA. These patterning effects are clearly observed in the oscilloscope traces shown in Fig. 5. These oscilloscope traces were measured by applying the 00001010

pattern to the wavelength conversion device in order to simply analyze a characteristic sampling of the signal. These traces show that in the RSF case patterning effects lead to a significant reduction in the power of the second '1' whereas these patterning effects are significantly reduced (almost negligible) in the case of BSF. This is because the probe spectral component shift to the high wavelengths (red chirp) happens at the same time as the gain compression by the pulse whereas the blue chirp occurs when the gain recovers, as shown in Fig. 2. Thus the amount of red chirp, on which the RSF technique is based, is largely more dependent on how well the gain has recovered than the blue chirp, on which the BSF technique is based. This will be explained in more detail in paragraph 4 with the aid of FROG characterisations and numerical results.

As shown in Fig. 6, these patterning effects lead to a small eye opening for the RSF case, while the BSF case retains a large eye opening, thus 80 Gbit/s error free performances can be achieved.

We can note that these observations are consistent with the results presented in the literature, demonstrating the RSF best performances at a bit rate not greater than 10 Gbit/s [19] and achieving high bit rate performances only with the BSF technique [12, 13, 17, 23, 27] or the combination of both techniques [24].

3.3 FROG characterisation

The converted pulses after each type of filtering and at each repetition rate of 10, 20, 40 and 80 GHz are now analyzed by the FROG technique [28]. The FROG setup consists of a second harmonic generation (SHG) autocorrelator followed by a high resolution spectrometer. For SHG, we used a $LiNbO_3$ crystal with an estimated interaction length of 250 μm. The SHG signal was spectrally resolved using a spectrometer with a charged coupled detector (CCD) array mounted on the output. The resulting spectrograms, which were obtained from the experimental FROG setup, were then used to retrieve the pulse intensity and phase using

the FROG phase retrieval algorithm of generalized projections (GP) [29]. For all the experimental results reported below, the transmission quality was checked with standard criteria, including inspection of the FROG frequency and delay margins, and comparing the spectrum and autocorrelation derived from the retrieved field with those directly measured. Pulse retrieval for the characterization carried out in this work, routinely gave low retrieval errors < 0.005 [29] with a 128x128 grid (i.e. 128 spectral and temporal points). This FROG measurement scheme overcomes the limitations of other pulse measurement schemes (such as autocorrelation or a photodiode in conjunction with an oscilloscope) which must make assumptions about the pulse shape and render no phase information.

The experimental setup remained the same as described above (in Fig. 3), however no data was applied to the intensity modulator, to obtain optimum pulse characterisation using the FROG technique. The FROG characterisation was carried out before any demultiplexing stage. Thus the analysis block comprises the SHG FROG preceded by an EDFA in order to obtain maximum sensitivity of the measurement scheme. This EDFA is designed specifically for short pulse amplification such that it does not introduce any chirp or alter the pulse shape.

The temporal profile of the pulses as measured by the FROG after red and blue shifted filtering at repetition rates of 10, 20, 40, and 80 GHz are displayed on Fig. 7, to examine how the repetition rate can affect the output pulse shape and chirp of the two wavelength conversion schemes [30].

While the measured pulses at these four repetition rates do not represent all the possible pulse variations that may be generated by patterning, they can give an overview of the wavelength converter behaviour as the bit rate is increased. Indeed it can be considered that the 80 GHz repetition rate corresponds to the case when the SOA's gain is maximally depleted, the 10 GHz repetition rate corresponds to the case where the gain has sufficient time

to completely recover between pulses while both 20 GHz and 40 GHz pulse represent two cases between these extremes.

This analysis shows that the wavelength converted pulses from the RSF technique are narrow, with a FWHM over the same time scale as the input pulse width (2 ps). This short pulse width looks very promising, that is why in Ref. [18], it has been shown that RSF gives optimum performance. However, this study does not take into account the bite rate dependence of the technique, which was observed thanks to BER measurements and has also been emphasized with the FROG analysis. Indeed the patterning effects resulting from going to higher bit rates are evident from the amplitude decrease in FROG traces taken with increasing input repetition rates.

In the case of BSF, illustrated in Fig. 7(b), the wavelength converted pulses are much broader; however the impact of patterning effects is far less evident as shown by the pulses being more independent of repetition rate. These assumptions will be confirmed thanks to the numerical study of the section 4. Nevertheless, the large pulse width around 7 ps after BSF may limit this type of wavelength conversion and could prevent from obtaining error free performance at bit rates greater than 80 Gbit/s.

The chirp following RSF and BSF is displayed in Fig. 8 and is overlaid on a normalized intensity profile (10 GHz). As expected, the resultant chirp is approximately linear as the changes in chirp after the SOA are converted into amplitude changes by the filtering. This would allow for the pulses to be compressed by using linear dispersion compensating techniques and thus could offer possibilities to transmit data at bit rates above 80 Gbit/s.

4 Numerical study and discussion

In order to a better understanding of the wavelength converter behaviour, leading to the observed different pulse shapes and patterning dependences, some numerical studies have

been carried on. A simple numerical model of the wavelength converter was constructed based on the SOA model proposed by Hong *et al.* [31]. The evolution of the electric field *E(t)* as it propagates through the SOA is given by equation (1). It is a function of the gain with variations due to carrier depletion g_N, which is given by equation (2), and the gain compression due to carrier heating and spectral hole burning $\Delta g_T(t)$, which is given by equation (3).

$$\left[\frac{\partial}{\partial z} - \frac{i}{2}\beta_2\frac{\partial^2}{\partial t^2}\right]E(t,z) = \left[\frac{1}{2}g_N(t)(1+i\alpha_N) + \frac{1}{2}\Delta g_T(t)(1+i\alpha_T) - \frac{\gamma}{2}\right]E(t,z) \tag{1}$$

$$g_N(t) = g_0 \exp\left(-\frac{1}{W_s}\int_{-\infty}^{\infty} u(t)\exp\left(-\frac{t}{\tau_1}\right)\left|E(t-\tau)\right|^2 d\tau\right) \tag{2}$$

$$\Delta g_T(t) = -\int_{-\infty}^{+\infty} u(t)\exp\left(-\frac{t}{\tau_2}\right)\left(h_1\left|E(t-\tau)\right|^2\right)d\tau \tag{3}$$

$$W_s = h\nu\frac{A}{\Gamma a} \tag{4}$$

Here, *u(t)* is the unit step function, while the other parameters are defined in Table 1. The saturation energy W_s is given by equation (4), where $h\nu$ is the photon energy. These equations are the same as those presented by Hong with some simplifications: We have chosen to neglect the two photon absorption and Kerr effect terms and the wavelength dependence of the gain because the influence of these factors was found to be negligible for pulse durations of the order of several picoseconds. Equation (2) has also been modified to allow for a finite carrier recombination lifetime τ_1, since the pulse duration and repetition period are of the same order as this time constant. Furthermore we decided to neglect the contribution of the amplified spontaneous emission as, in the experiment, the involved input pulse powers are high and the ASE was thus saturated. For a more complete SOA model which incorporates all these factors the reader is directed to the work of Wang et *al.* [23]. Equations (1)-(3) were used to simulate the experimental setup outlined in Section 2. The both filter shapes were modelled and combined like in the experimental setup. The resulting

temporal profiles of the wavelength converted pulses for the two filtering configurations and the four repetition rates are given in Fig. 9. When compared to the experimental results given in Fig. 7, these simulations show good qualitative agreement.

Two main factors influence the shape and amplitude of the wavelength converted pulses. Firstly the magnitude of the SOA induced frequency chirp which combined with the filter profile controls the time dependant filter transmission. This is expressed in the model through the phase modulation imparted by the alpha parameters α_N and α_T. Secondly the SOA's time varying gain which is experienced by the CW probe also affects the output pulse shape. This is given by the real parts of g_N and Δg_T in equation (1). The SOA induced chirp and the corresponding gain responses at the different studied repetition rates are plotted on Fig. 10 thanks to the numerical model. This figure clearly shows the patterning effects induced on the gain (which is well-known) and the chirp. What can be pointed out is that the amount of red chirp is influenced by patterning effects whereas the level of blue chirp remains quite constant whatever the repetition rate. As it indeed turns out, the red chirp corresponds to the gain compression (as it is shown on Fig. 2) and thus if the compression rate changes due to patterning effects, consequently the amount of red chirp varies. On the contrary, the blue chirp is linked to the gain recovery (cf Fig. 2), which does not depend on patterning effects. Furthermore the blue chirp takes advantages of intra-band effects which decrease nonlinear patterning dependence [25].

These explanations lead to a better understanding of wavelength converted pulse shapes in case of RSF and BSF techniques.

The RSF pulses depend on the fast gain saturation effect that occurs approximately over the pulse width of the input pulse (2 ps). Due to this fast depletion of carriers the corresponding red chirp, which occurs over the same time scale, causes the spectral

components of the wavelength converted probe signal to shift to longer wavelengths. This allows only these spectral components to pass through the filter thus outputting a very short pulse as can be seen in Fig. 7(a) and Fig. 9(a). However, the amount of red chirp depends on the carrier density and thus on the carrier lifetime. Consequently, if there is not a complete gain recovery before the onset of the next pulse, there is a smaller red shift of the probe and thus there is less power output from the filter. Therefore the major drawback of RSF is the patterning effects resulting from going to higher bit rates, as is evident from the amplitude decrease in FROG traces or numerical results taken with increasing input repetition rates as well as from the previous BER measurements.

In BSF technique, as the blue chirp is smaller than the red chirp, because the phase recovers over a longer timescale, the wavelength converted pulses are longer than the RSF case, which is confirmed in both experimental and theoretical results. One can also note that, in contrast to the red chirp, the model shows that the magnitude of blue frequency chirp increases slightly with repetition rate, as demonstrated on Fig. 10. In the case of BSF this means that for a carefully positioned filter, the filter's transmission increases when the pulse separation is decreased. This has also been noted in [24] where it was used to balance the patterning of the RSF. However, for the single BSF technique used here the patterning can also be reduced, using the fact that while the BSF filter transmission increases with repetition rate the gain decreases. These two opposite effects can, to some extent, be balanced thereby leading to a much more repetition rate independent output pulse as shown in Fig. 7(b) and Fig. 9(b). To sum up, by tuning the central frequency of the optical filter in the model we found that if the filter is too close to the central component of the probe the amplitude of the output pulses decreased with increasing repetition rate implying that the SOA gain dynamics were the dominant effects. Conversely if the filter was too far away from the probe central component, the pulses amplitudes increased with increasing repetition rate implying that the

SOA chirp dynamics (and filter transmission) are the dominant processes. Fig. 7(b) and Fig. 9(b) represent a more optimal filter position where the two processes are of similar magnitude.

5 Conclusion

We have presented a large analysis of pulses obtained thanks to an SOA-based shifted filtering wavelength conversion scheme. By placing a filter so as to suppress the central component of the probe following the SOA, polarity preserved wavelength conversion can be achieved. Back-to-back system performance was analyzed and it showed that placing the filter to retain the blue spectral components can give error free performance up to 80 Gbit/s. Characterisation of both the RSF and BSF was carried out using the FROG measurement technique, which showed that the pulse shape is largely dependent on the input data pattern. These experimental results were confirmed by a numerical study which allowed to further explain the experimental observations. In the case of the RSF, short pulses can be obtained but there is a large patterning due to the slow gain recovery time of the SOA whereas with the BSF technique, patterning effects are significantly reduced.

Acknowledgments

G. Girault would like to thank O. Vaudel for helpful advice and fruitful discussions and M. and I. Joindot for their critical reading of the manuscript. This work was supported in part by the Enterprise Ireland, Science Foundation Ireland, the Research Ministry of France, the Britanny Region and the European Commission (FEDER).

References

[1] S. J. B. Yoo, J. Lightwave Technol. 14 (June 1996) 955.

[2] M. Asghari, I. H. White, R. V. Penty, J. Lightwave Technol. 15 (July 1997) 1181.

[3] N. K. Dutta and Q Wang, "Semiconductor optical amplifiers" (World Scientific Publishing Co. Pte. Ltd.), Feb. 2006.

[4] C. Holtman, ECOC We (1998) 499.

[5] P. Doussière, P. Garabedian, C. Graver, D. Bonnerie, T. Fillion, E. Derouin, M. Monnot, J. G. Provost, D. Leclerc, M. Klenk, Photon. Technol. Lett. 6 (Feb 1994) 170.

[6] T. Durhuus, B. Mikkelsen, C. Joergensen, S. L. Danielsen, K. Stubkjaer, J. Lightwave Technol. 14 (1996) 942.

[7] D. Nesset, T. Kelly, D. Marcenac, IEEE Commun. Mag. 36 (Dec 1998) 56.

[8] P. B. Hansen, J. M. Wiesenfeld, G. Eisenstein, R. S. Tucker, G. Raybon, J. Quantum Electron. 25 (Dec 1989) 2611.

[9] Y. Ueno, S. Nakamura, J. Sasaki, T. Shimoda, A. Furukawa, T. Tamanuki, T. Sasaki, K. Tajima, ECOC Th.F.2.1 (Sept 2001).

[10] J. Leuthold, C. H. Joyner, B. Mikkelsen, G. Raybon, J. L. Pleumeekers, B. I. Miller, K. Dreyer, C. A. Burrus, Electron. Lett. 36 (June 2000) 1129.

[11] Y. Liu, M. T. Hill, E. Tangdiongga, H. de Waardt, N. Calabretta, G. D. Khoe, H. J. S. Dorren, Photon. Technol. Lett. 15 (Jan 2003) 90.

[12] A.D. Ellis, A.E. Kelly, D. Nesset, D. Pitcher, D.G. Moodie, R. Kashyap, Electron. Lett. 34 (1998) 1958

[13] Y. Liu, E. Tangdiongga, Z. Li, H. de Waardt, A. M. J. Koonen, G. D. Khoe, H. J. S. Dorren, X. Shu, I. Bennion, OFC, PDP28 (2005).

[14] P. Cho, D. Mahgerefteh, J. Goldhar, G. L. Burdge, Photon. Technol. Lett. 10 (Jan 1998) 66.

[15] P. Mamyshev, ECOC (1998) 475.

[16] B-E. Olsson, P. Ohlen, L. Rau, D. Blumenthal, Photon. Technol. Lett. 12 (July 2000) 846.

[17] M. L. Nielsen, Electron. Lett. 39 (Sept 2003) 1334.

[18] S. Fu, J. Dong, P. Shum, L. Zhang, X. Zhang, and D. Huang, Optics Express 14 (2006) 7587.

[19] H. Chayet, S.B. Ezra, N. Shachar, S. Tzadok, S. Tsadka, J. Leuthold, OFC 2 (2004) 23.

[20] M. Nielsen, J. Mork, J. Sakaguchi, R. Suzuki, Y. Ueno, OFC OThE7 (2005).

[21] J. M. Vazquez, Z. Li, Y. Liu, E. Tangdiongga, S. Zhang, D. Lenstra, G. D. Khoe, H. J. S. Dorren, J. Quantum Electron. 43 (Jan 2007) 57.

[22] Y. Liu, E. Tangdiongga, Z. Li, S. Zhang, H. de Waardt, G. D. Khoe, H. J. S. Dorren, J. Lightwave Technol. 24 (Jan 2006) 230.

[23] J. Wang, A. Maitra, C. G. Poulton, W. Freude, J. Leuthold, J. Lightwave Technol. 25 (March 2007) 891.

[24] A. Marculescu, J. Wang, J. Li, P. Vorreau, S. Zadok, S. Ben Ezra, S. Tsadka, W. Freude, J. Leuthold, ECOC (2007).

[25] M. L. Nielsen, J. Mork, R. Suzuki, J. Sakaguchi, Y. Ueno, Opt. Express. 14 (2006) 331.

[26] R. J. Manning, D. A. O. Davies, Opt. Lett. 19 (June 1994) 889.

[27] L. Bramerie, A. Clarke, G. Girault, S. Lobo, M. Gay, C. Guignard, V. Roncin, B. Kennedy, P. Maguire, S. Fève, B. Clouet, F. Ginovart, L. P. Barry, J.C. Simon, CLEO/QELS CMT7 (2006).

[28] R. Trebino, K. W. Long, D. N. Fittinghoff, J. N. Sweetser, M. A. Krumbugel, B. A. Richman, Rev. Sci. Instrum. 68 (1997) 3277.

[29] D.J. Kane, J. of Selected Topics in Quantum Electronics 4 (1998) 278.

[30] A. Clarke, G. Girault, P. Anandarajah, C. Guignard, L. Bramerie, L. Barry, J-C. Simon and J. Harvey, LEOS MP 2 (2006).

[31] M. Y. Hong, Y. H. Chang, A. Dienes, J. P. Heritage, and P. J. Delfyett, J. Quantum Electron. 30 (1994) 1122.

Table Captions

Table 1: SOA parameters used in the numerical study.

Figure Captions

Fig.1. Principle of wavelength converter based on cross phase modulation (XPM) in a SOA associated with a shifted bandpass filter (BPF).

Fig.2. Time correspondences between input pump pulse, SOA gain compression and induced SOA chirp.

Fig.3. Experimental setup.

Fig.4. Signal spectra at different points of the experimental wavelength conversion process at 80 GHz: at the SOA input (a), at the SOA output (b), wavelength converted signal after RSF (c), wavelength converted signal after BSF (d).

Fig.5. 80 Gbit/s signal analysis for each case of filtering (BSF or RSF): BER measurements versus the received power and associated oscilloscope traces for the 00001010 pattern (only the four last symbols are displayed).

Fig.6. Experimental eye diagrams of the wavelength converted signal at 80 Gbit/s following (a) RSF and (b) BSF for a power received of -7.5 dBm relating to a BER of $\sim 10^{-7}$ and 10^{-9} for RSF and BSF respectively.

Fig.7 Experimental temporal pulse profiles at different repetition rates after (a) RSF and (b) BSF.

Fig.8. Normalized intensity profile (10 GHz) and experimental chirp profiles at different repetition rates in case of (a) RSF and (b) BSF.

Fig.9. Numerical temporal pulse profiles at different repetition rates after (a) RSF and (b) BSF.

Fig.10. Simulation of the patterning effects on the SOA gain and chirp.

Table

Table 1: SOA parameters used in the numerical study.

Symbol	**Parameter**	**Value**
W_s	Saturation energy	3.14×10^{-12} J
τ_1	Carrier lifetime	55 ps
τ_2	Carrier-heating lifetime	500 fs
h_1	Contribution of carrier-heating to gain reduction	0.14×10^{17} J^{-1}
g_0	Linear gain	10100 m^{-1}
β_2	Group velocity dispersion	1×10^{-24} $s^2 m^{-1}$
α_N	Alpha parameter for carrier recombination	5.5
α_T	Alpha parameter for carrer heating	0.3
γ	Linear losses	1150 m^{-1}
A	SOA cross-sectional area $(A = w \times l)$	2.45×10^{-13} m^2
L	SOA length	800×10^{-6} m
Γ	Confinement factor	0.5
a	Gain coefficient	2×10^{-20} m^{-2}

This table presents the different parameters involved in the equations of the used SOA model. The symbols are those used in the different equations described in the paper. This table also shows the chosen value for these parameters.

first figure

Click here to download high resolution image

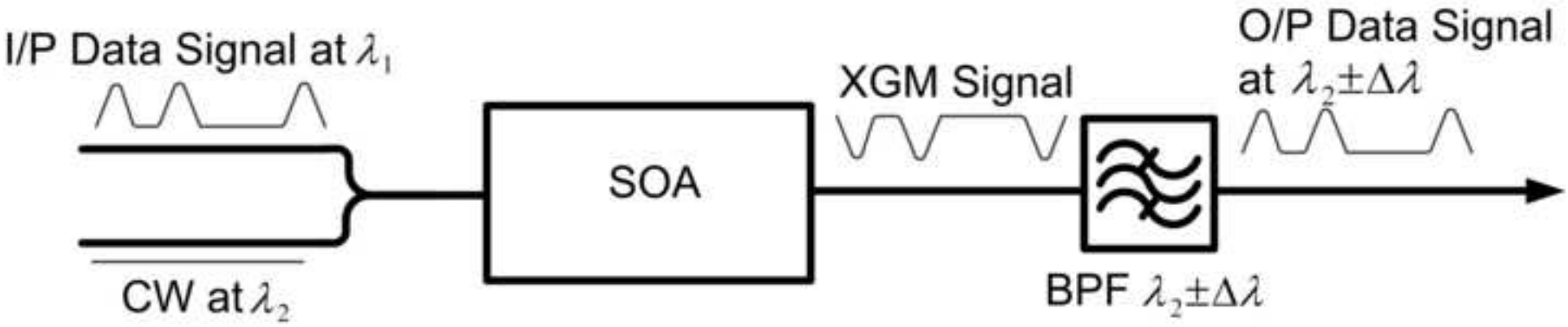

second figure

Click here to download high resolution image

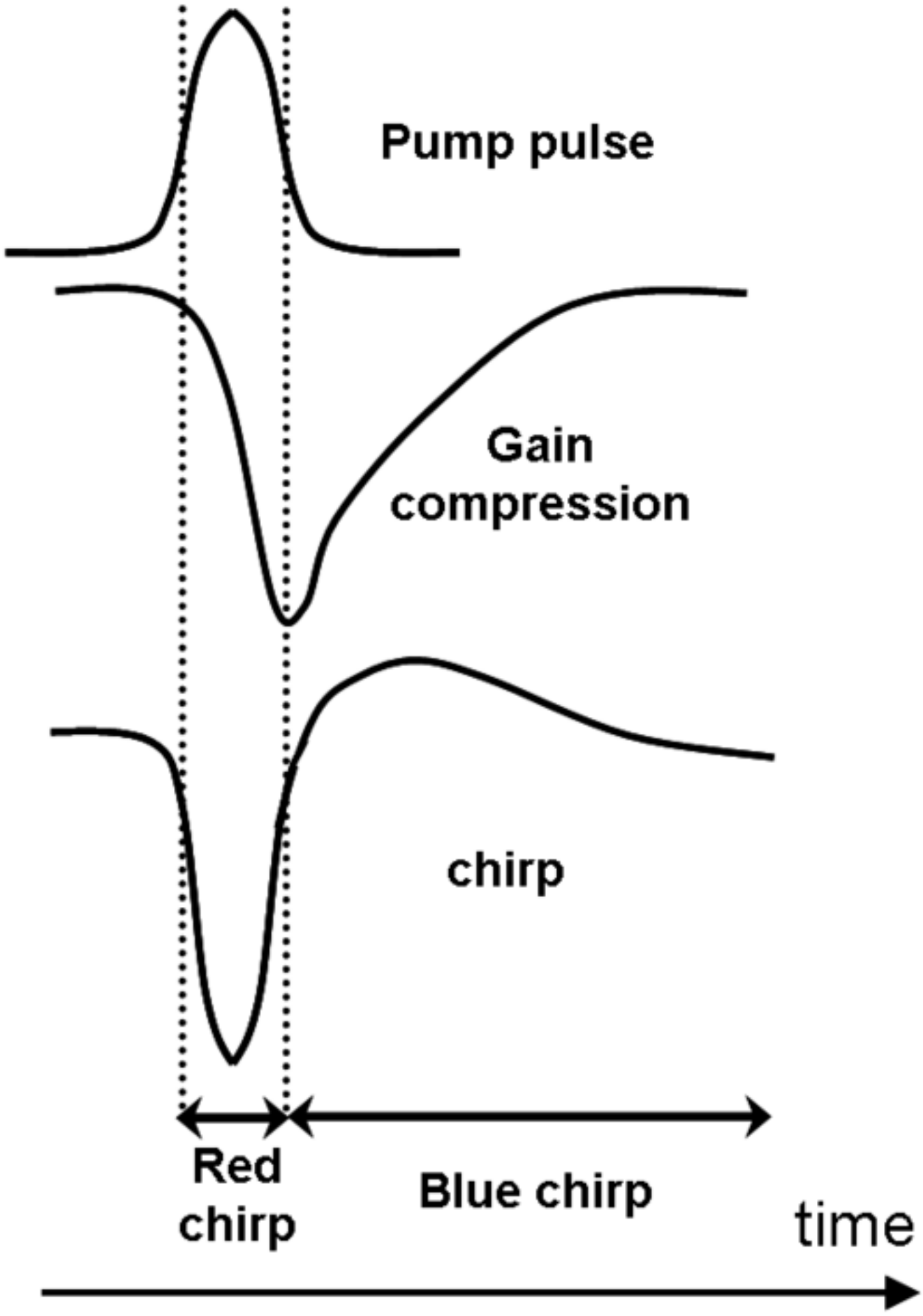

third figure

Click here to download high resolution image

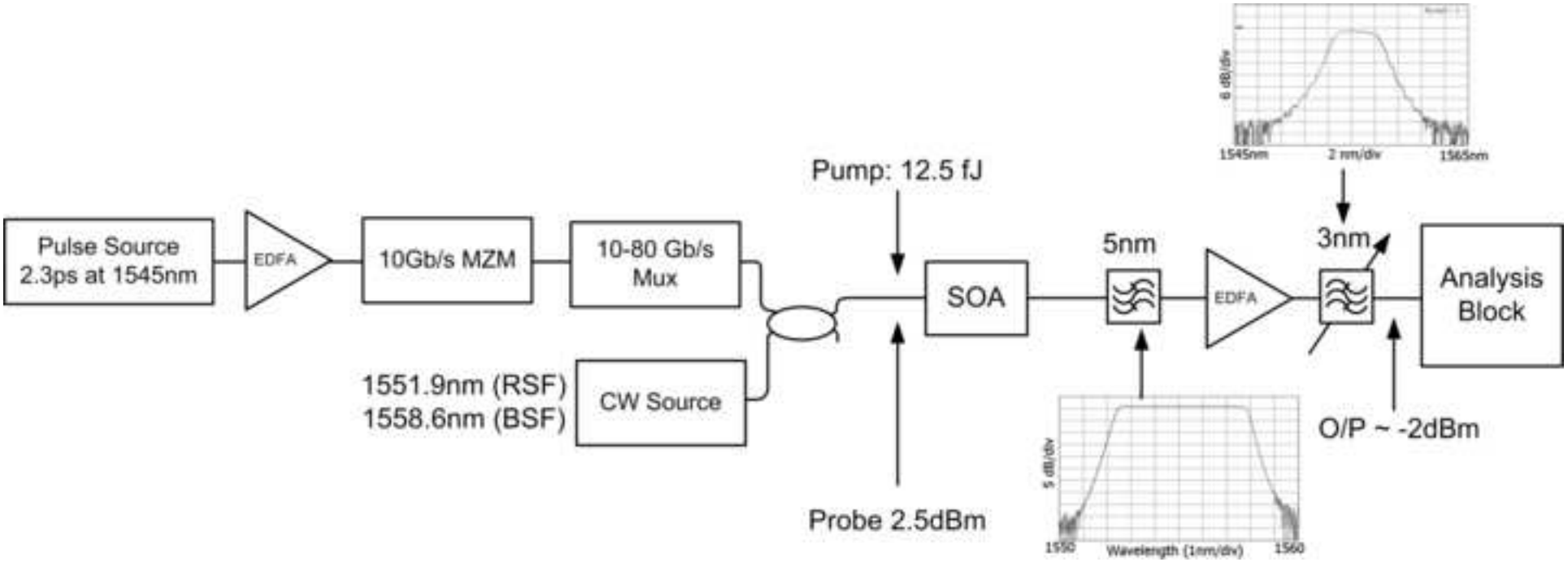

fourth figure

Click here to download high resolution image

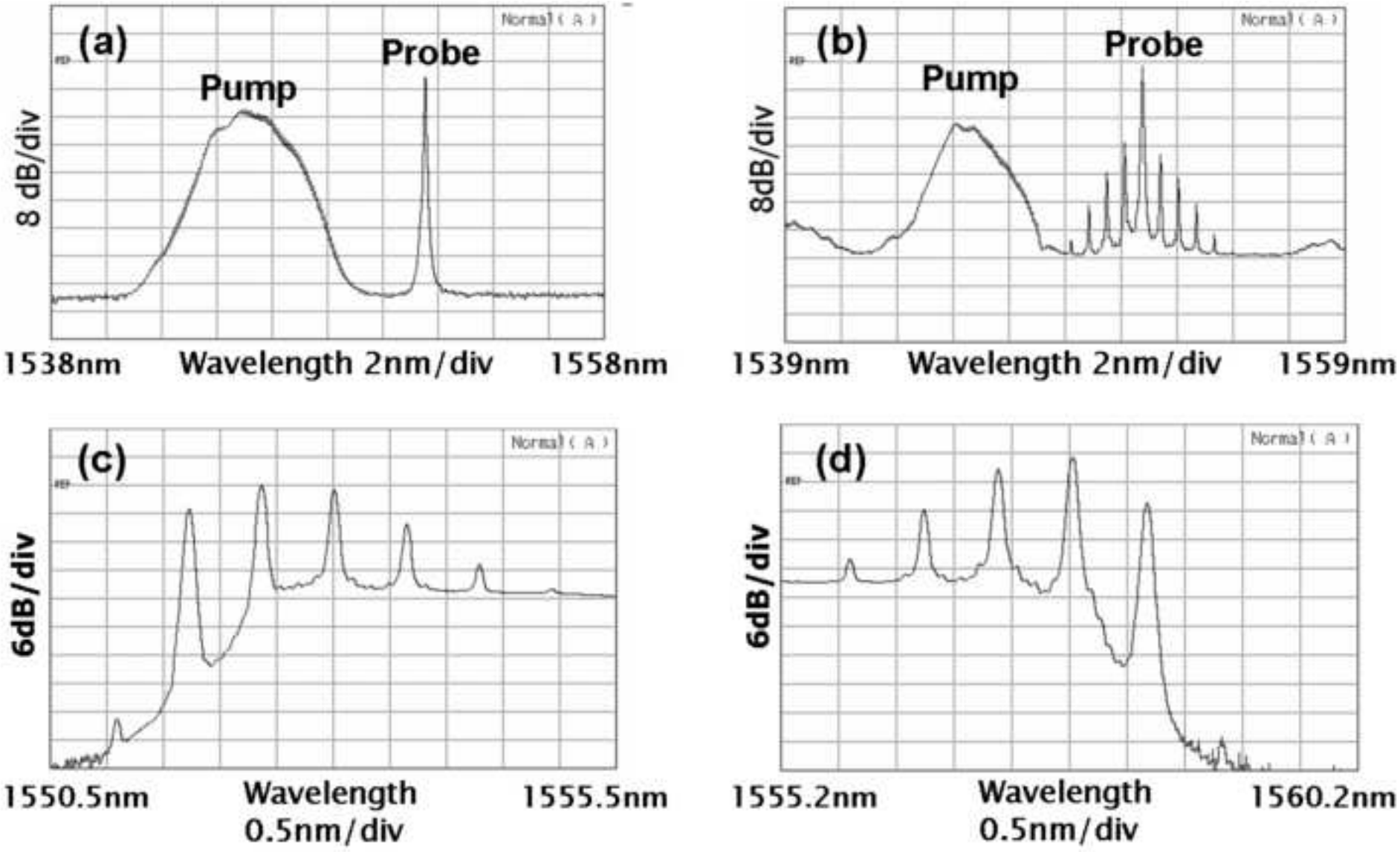

fifth figure

Click here to download high resolution image

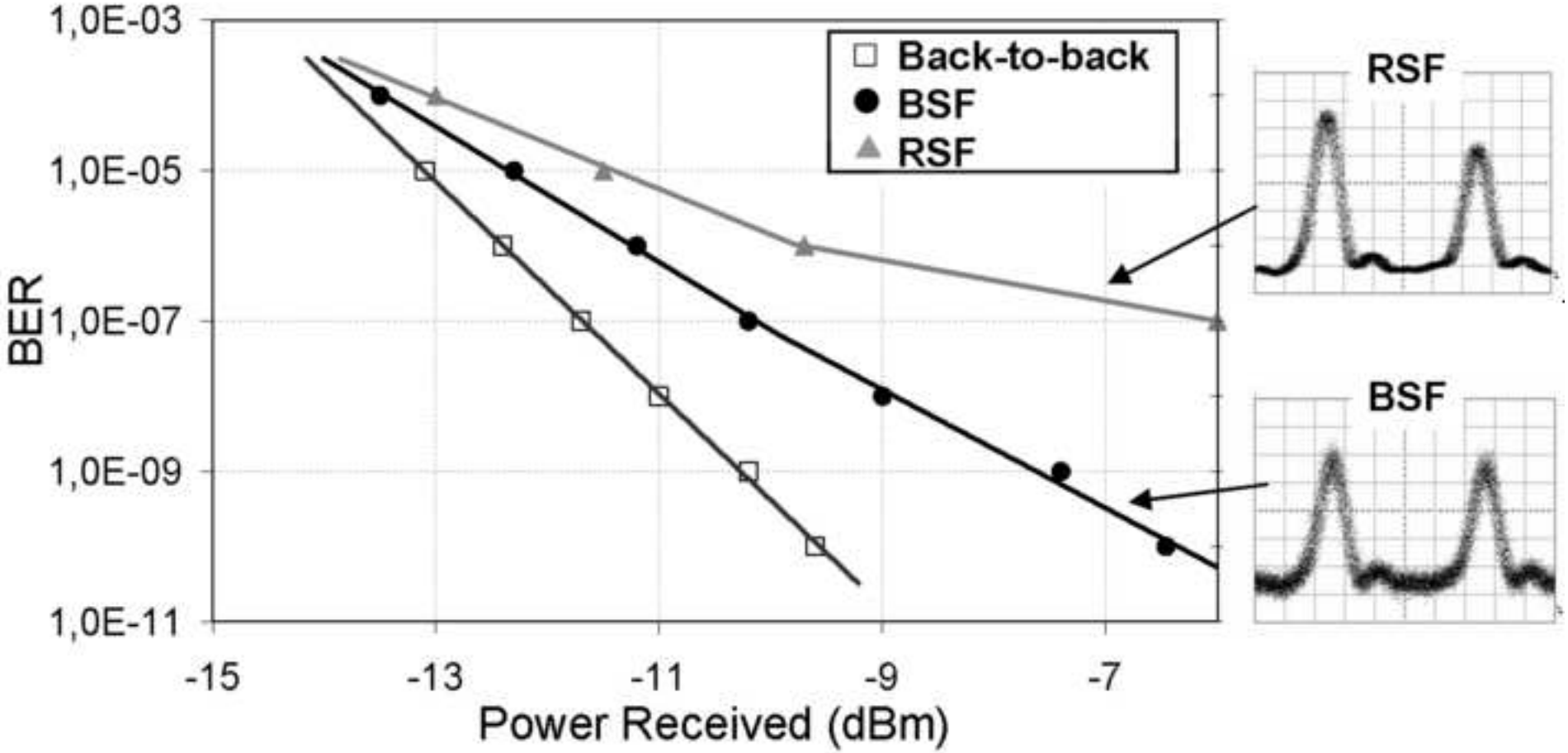

sixth figure

Click here to download high resolution image

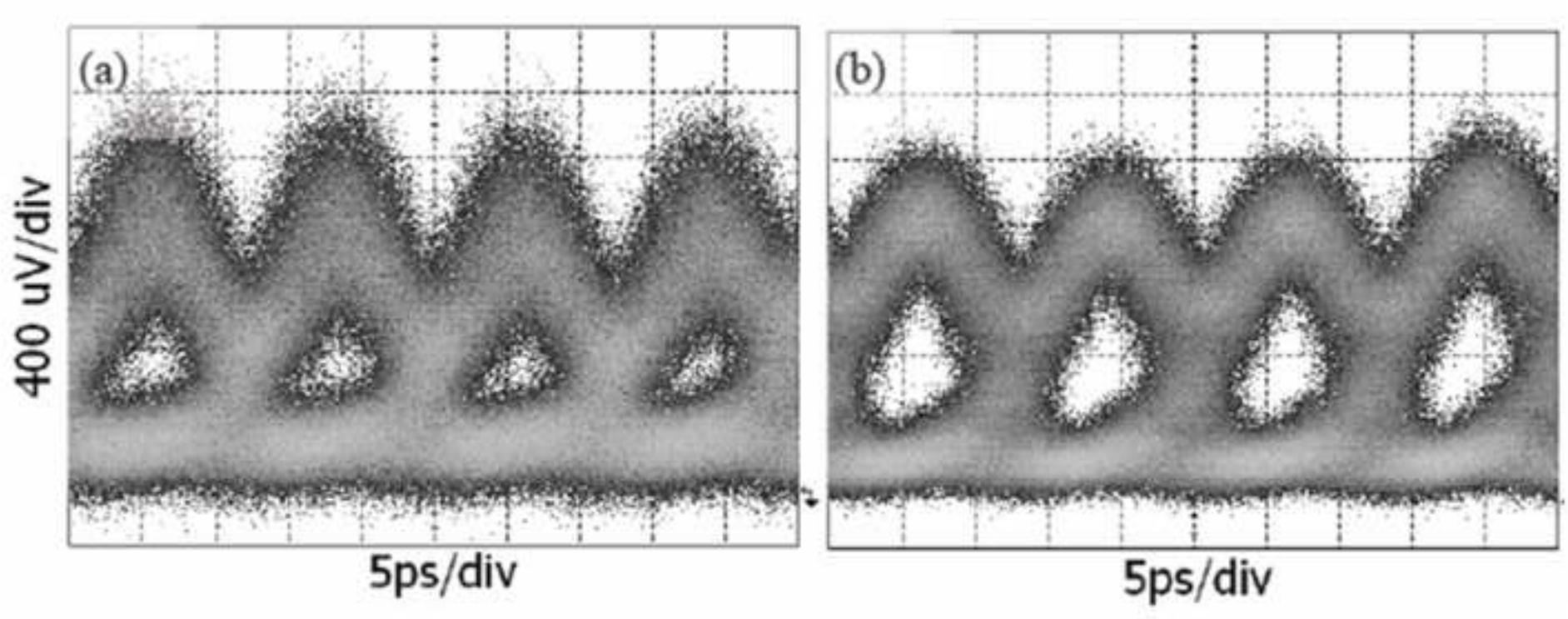

seventh figure

Click here to download high resolution image

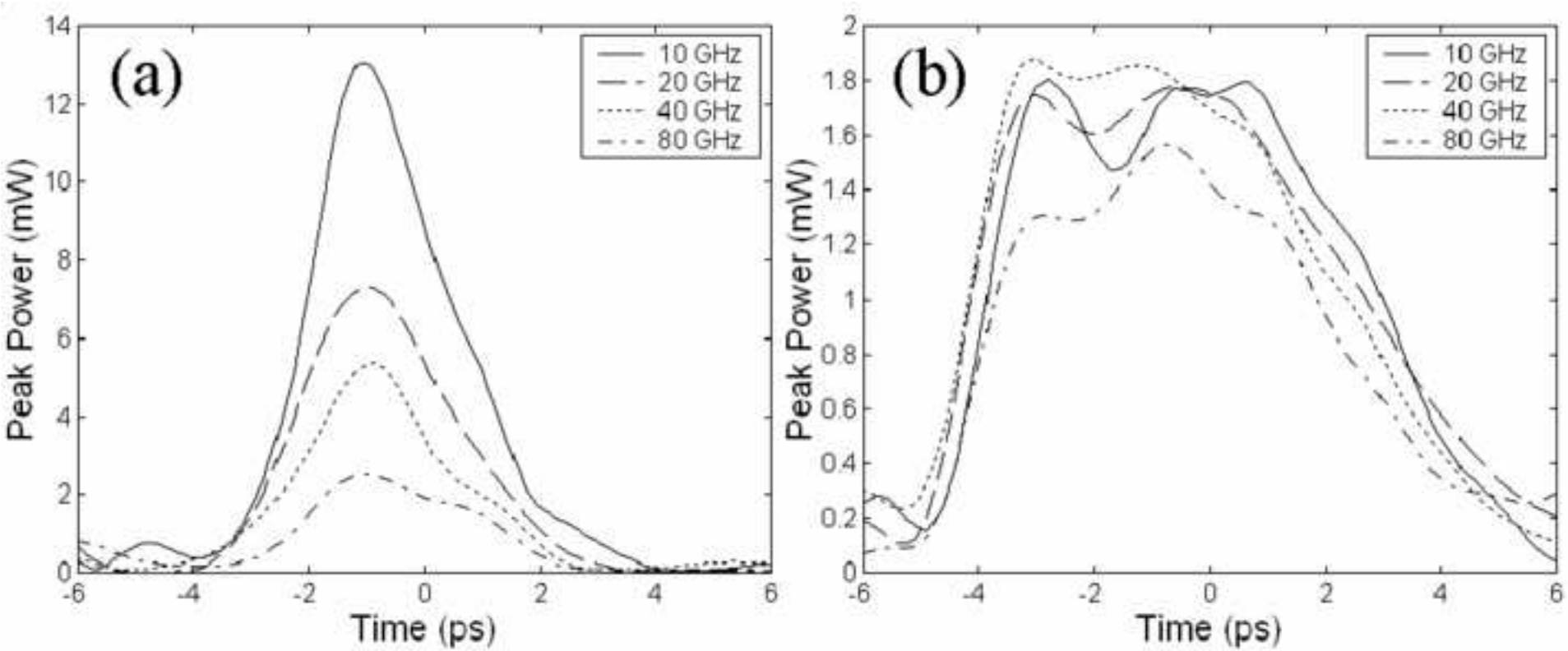

eighth figure

Click here to download high resolution image

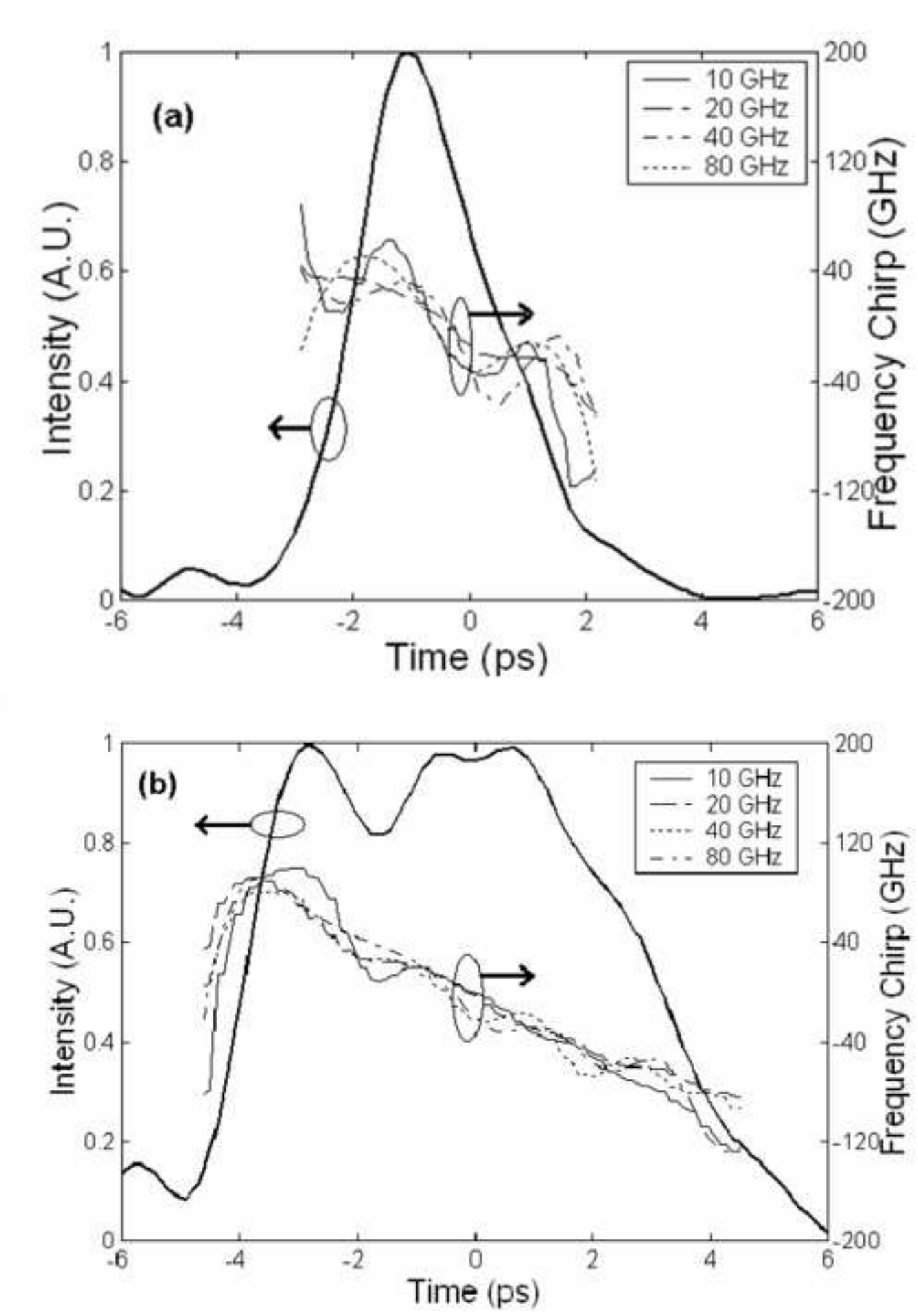

ninth figure

Click here to download high resolution image

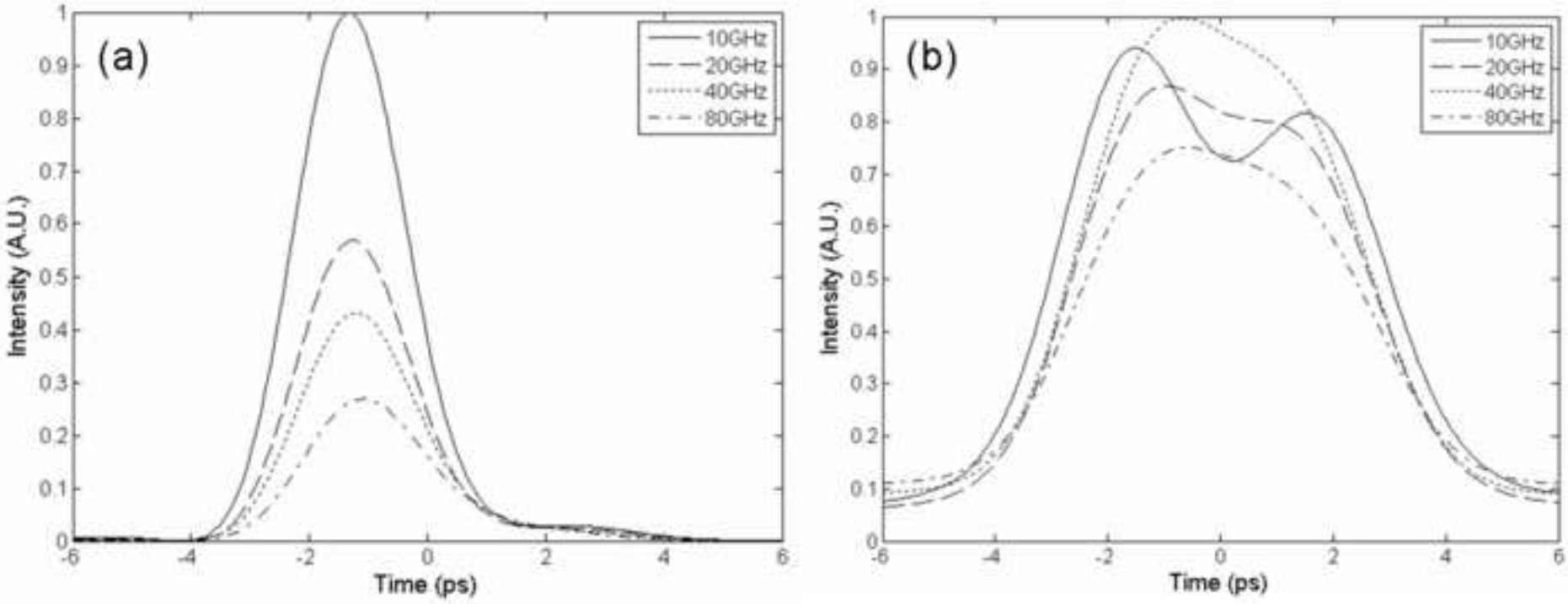

tenth figure
Click here to download high resolution image

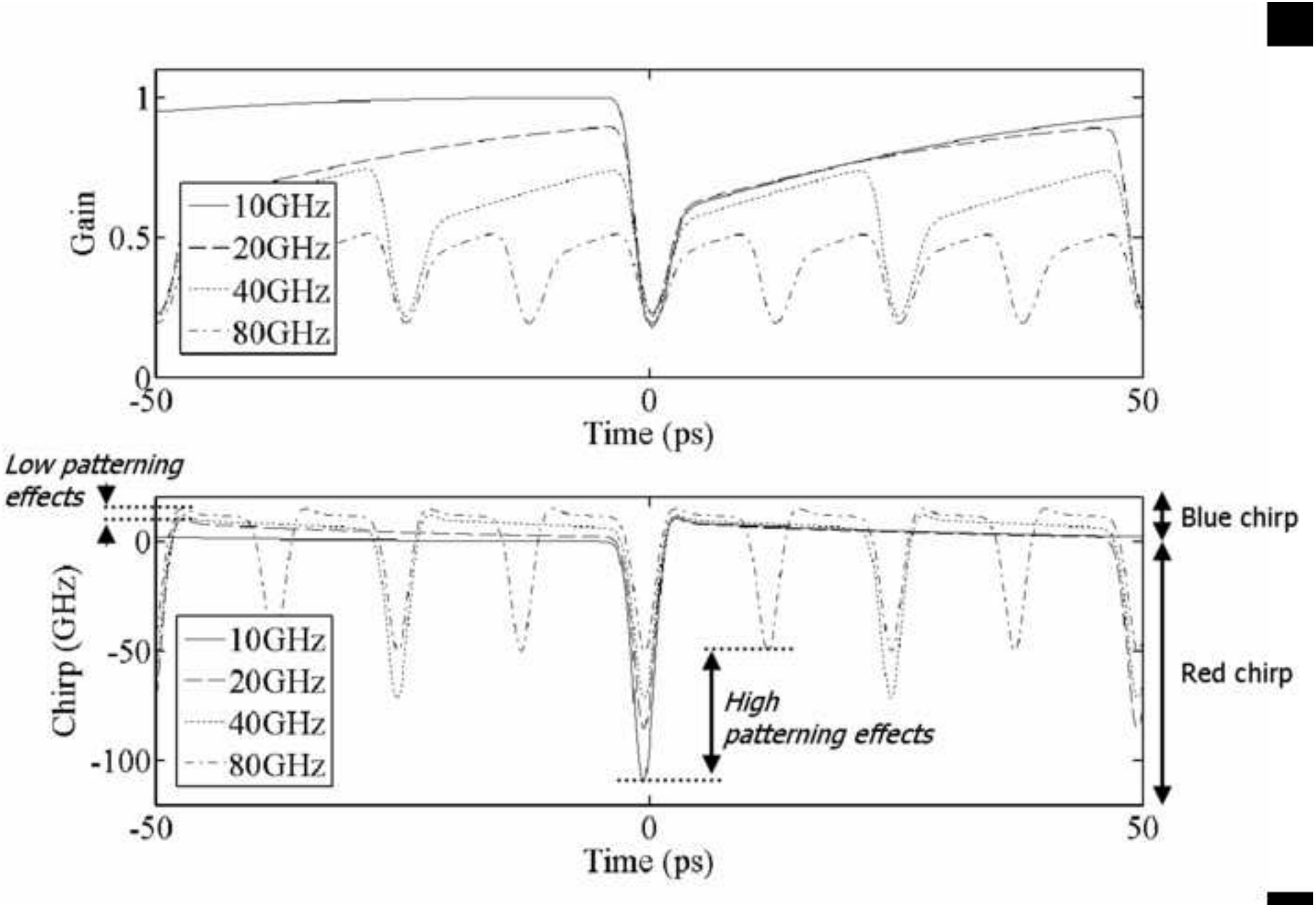

Lannion, 13th August 2008

Dear Editor,

Please find our submission to Optics Communications. This paper is entitled "Analysis of bit rate dependence up to 80 Gbit/s of a simple wavelength converter based on XPM in a SOA and a shifted filtering" and the authors are Gwenaëlle Girault, Aisling Clarke, Douglas Reid, Céline Guignard, Prince Anandarajah, Laurent Bramerie, Liam Barry, Jean-Claude Simon and John Harvey from the laboratories CNRS Foton-Enssat in Lannion (France), RINCE in Dublin (Ireland) and Auckland University (New Zealand).

This paper deals with the study of a simple wavelength converter based on cross phase modulation in a semiconductor optical amplifier in conjunction with a shifted filtering allowing data polarity preservation and operating at high bit rates up to 80 Gbit/s. We provide a analysis of wavelength converted pulses obtained thanks to the proposed scheme including experimental BER measurements of the back-to-back system performance as well as a frequency-resolved optical gating (FROG) characterization. This allows us to compare system performance and wavelength converted pulse shapes for both red and blue shifted filtering. These experimental results are supported by a numerical study which helps to achieve a better understanding of the roles of the involved physical phenomena. The placement of the filter to undertake blue shifted filtering shows optimum performance in comparison to red shifted filtering as regards to patterning effects at high bit rate.

Best regards,

The authors.